Chapter IV

RESULTS AND DISCUSSION

CHAPTER IV

Results and Discussion

4.1	**Introduction**		48
4.2	**Results and Discussion**		48
	4.2.1	X-ray diffraction	48
	4.2.2	Scanning electron microscopy	52
	4.2.3	Dielectric measurements	52
	4.2.4	Electrical resistivity	55
	References		58

4.1 Introduction

Recently there has been great attention for investigating new gas-sensing materials and developing the properties of known gas-sensing materials. Most of these materials are metal oxides. Cadmium stannate shows quite attractive electrical properties [1-2]. Advantages of oxides for gas detections are high sensitivity, simple design, and low weight and cost. Recently synthesis and gas sensing properties of perovskite $CdSnO_3$ nanoparticles have been reported by Jia et al. [3]. $CdSnO_3$ nanoparticles were prepared by a chemical co-precipitation method and studied the selectivity to vapours of C_2H_5OH. Cd_2SnO_4, being one of the alternatives to the present generations transparent conducting oxides (TCOs); FTO and ITO, is synthesized in thin film form by various techniques [4-5]. Nozik [6] prepared Cd_2SnO_4 amorphous thin films and studied electrical and optical properties. Hashemi [7] has employed investigation of chemical nature of samples of Cd_2SnO_4 in as–fired and electrochemically reduced and reoxidised states. Valincius et al. [8] reported the electrochemical properties of Sol-gel prepared nano-crystalline electrodes of cadmium tin oxide films.

We present here the formation of different powder samples in the Cd-Sn-O system by co-precipitation method having enhanced dielectric properties.

4.3 Results and discussion

4.3.1 X-ray diffraction

X-ray diffraction patterns of cadmium stannate samples sintered at different temperatures are shown in figure 4.1. The samples are polycrystalline and fit well with the rhombohedral and spinel cubic crystal structures with preferred characteristic temperatures. The intensity and number of diffraction peaks depend on the amount of corresponding phases. The data was analyzed by making use of JCPDS card Nos. 34-

0758 (rhombohedral $CdSnO_3$), 80-1469 (spinel cubic Cd_2SnO_4) and 73-0973 (spinel cubic $Cd_{1.33}Sn_{1.33}O_4$).

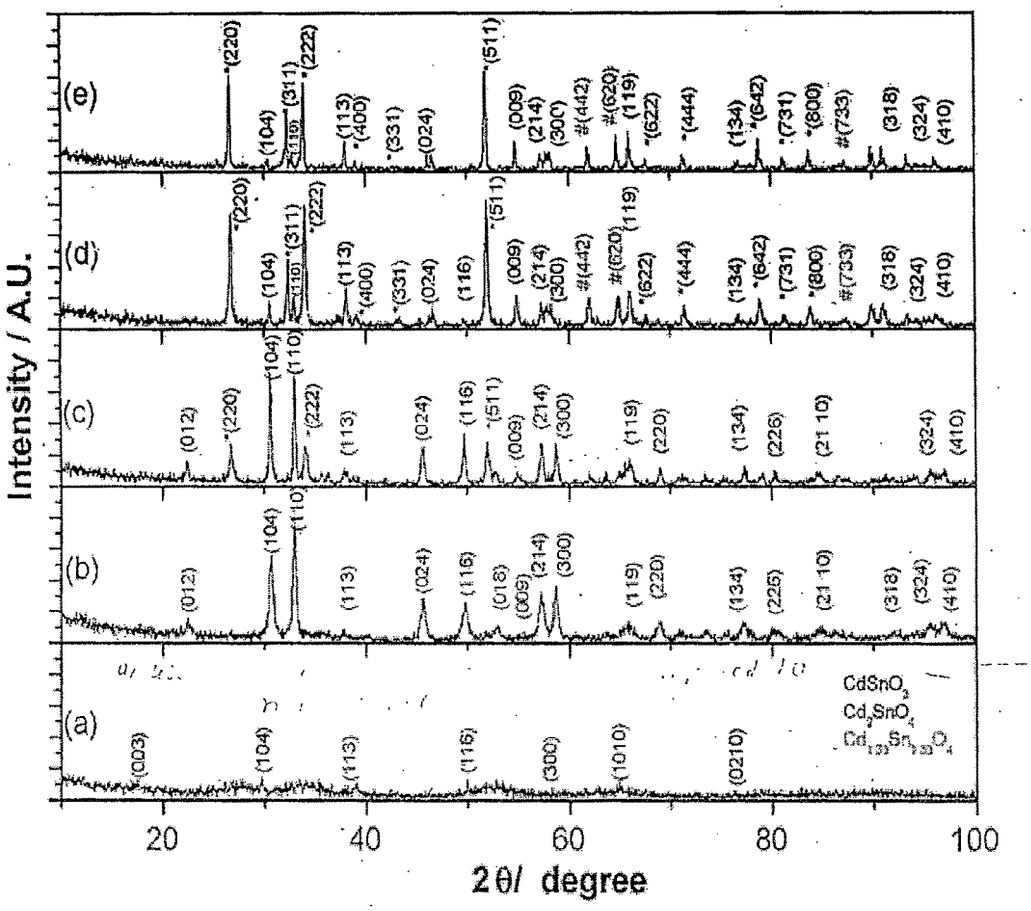

Figure 4.1 X-ray diffraction patterns of cadmium stannate samples annealed at different temperatures; (a) 400°C, (b) 600°C, (c) 800°C, (d) 1000°C and (e) 1200°C

At 400°C sample shows an amorphous as well as the nanocrystalline $CdSnO_3$ phase. At 600°C the XRD pattern shows rhombohedral crystal structure with only $CdSnO_3$ phase and all the peaks could be easily identified. Sample sintered at 800°C shows strong presence of $CdSnO_3$ phase. But the presence of (220), (222) and (511) peaks from Cd_2SnO_4 phase confirms that it is changing to Cd_2SnO_4 phase. At higher temperatures viz. 1000 and 1200°C the sample show mixed phases of $CdSnO_3$, Cd_2SnO_4 and $Cd_{1.33}Sn_{1.33}O_4$. The (222) and (511) planes of Cd_2SnO_4 spinel cubic structure are

observed to be strongest in the sample sintered at 1000°C (d_{222}=2.6359 Å) and 1200°C (d_{511}=1.7672 Å) respectively. The shifting of strongest plane in the sample sintered at 1200°C sample with respect to that of the one sintered at 1000°C is due to change in single crystal d value. The other planes such as (311), (331), (400), (444), (622), (642), (731) and (800) are observed for Cd_2SnO_4 phase. Another new phase $Cd_{1.33}Sn_{1.33}O_4$ having (442), (620) and (733) planes is observed in spinel cubic crystal structure. As the sintering temperature increases up to 800°C the peak intensity of $CdSnO_3$ phase increases. In case of Cd_2SnO_4 phase it increases as the temperature is raised up to 1000°C because of enhancement in crystallinity. It then decreases due to the crystal reorientation effect. Table 4.1 gives comparison of standard and observed d value for Cd-Sn-O system.

Table 4.1 Comparison of standard and observed'd' values for co–precipitated cadmium stannate samples

(hkl) planes for phase		Std. 'd' value	Observed 'd' values for the samples annealed at various temperatures (^{0}C)				
$CdSnO_3$	Cd_2SnO_4		400	600	800	1000	1200
(003)		5.033	5.0521				
(012)		3.996	-	3.9730	3.9765	-	-
	(220)	3.2435	-	-	3.3282	3.3412	-
(104)		2.932	2.9976	2.9222	2.9250	2.9250	-
	(311)	2.7660	-	-	-	2.7657	2.7778
(110)		2.726	-	2.7213	2.7213	-	-
	(222)	2.6483	-	-	2.6419	2.6359	-
(113)		2.394	2.3153	-	2.3748	2.3643	2.3715
	(400)	2.2935	-	-	-	-	2.3102
	(331)	2.1046	-	-	-	-	2.1119
(024)		1.996	-	-	1.9979	2.0951	-
	(511)	1.7655	-	-	-	1.7636	1.7672
	(440)	1.6217	-	-	-	-	1.6103
	(531)	1.5506	-	-	-	-	1.5859
(116)		1.840	1.8306	1.8344	1.8368	-	-
(018)		1.737	-	1.7356	1.7631	-	-
(009)		1.662	-	-	1.6700	1.6737	-
(214)		1.610	1.5855	1.6134	1.6073	1.6086	-
(442)	$Cd_{1.33}Sn_{1.33}O_4$	1.5251	-	-	-	1.5139	-

hkl planes for phase		Std. 'd' value	Observed 'd' values for the samples annealed at various temperatures (^{0}C)				
$CdSnO_3$	Cd_2SnO_4		400	600	800	1000	1200
(010)		1.4270	1.4374			1.1470	
	(534)	1.3990	-	-	3.973	1.3857	1.3893
(306)		1.3300	-	-	-	-	1.3252
	(444)	1.3241	-	-	-	1.3238	1.3252
(300)		1.573	-	1.5764	1.5728	-	-
(119)		1.420	-	1.4219	1.1484	-	-
(220)		1.362	-	1.3644	1.3615	-	-
(128)		1.290		1.2897	1.2969	-	-
(134)		1.236	1.2501	1.2362	1.2372	1.2452	1.2463
	(642)	1.2259	-	-	-	1.2134	-
(226)		1.196	-	1.2000	1.1965	1.1822	-
(410)		1.030	-	1.0289	1.0307	1.0336	
	(800)	1.1467	-	-	-	1.1557	1.1541
(404)		1.1260	-	-	-	-	1.1204
(229)		1.0540	-	-	-	-	1.060
(318)		1.0720	-	-	-	1.0802	-
(2110)		1.146	-	1.1459	1.1462	-	-
(324)		1.040	-	1.0400	1.0423	1.0509	1.0359

4.3.2 Scanning Electron Microscopy

Fig. 4.2 shows SEM micrographs of Cd_2SnO_4 sample sintered at 1000°C. The SEM studies reveal a compact morphology with large number of particles. This may be the unique feature of this material that such a large number of small particles are formed when the sintering of material occurs.

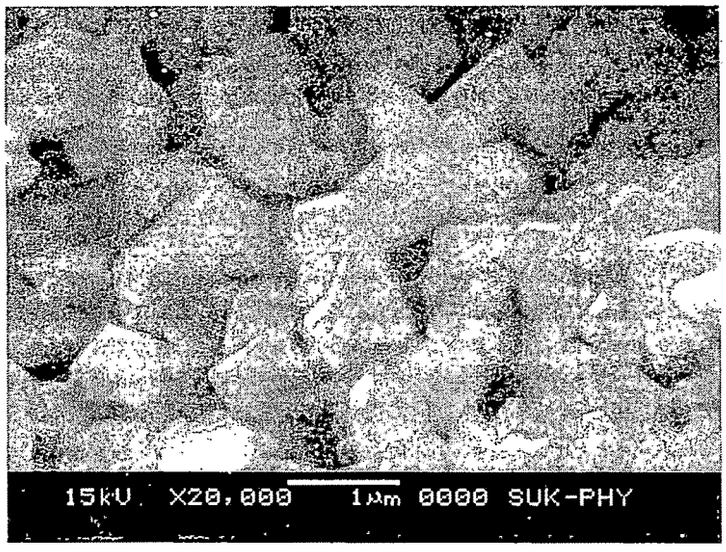

Figure 4.2 Scanning electron micrograph of Cd_2SnO_4 sample sintered at 1000°C magnification: 20,000X

4.3.3 Dielectric measurements

The variation of dielectric constant with frequency at room temperature for the samples is shown in fig. 4.3. From the figure it is clear that dielectric constant (ε') decreases abruptly at lower frequencies and remains constant at higher frequencies

increases

showing dispersion of dielectric constant at lower frequencies. The dielectric constant varies with applied frequency due to charge transport relaxation time. This dielectric dispersion is attributed to Maxwell [9] and Wagner [10] type of interfacial polarization in agreement with Koop's phenomenological theory [11]. Since polarization decreases with increasing frequency and reaches constant values, decrease in dielectric constant with frequency is observed. The large value of dielectric constant is associated with space charge polarization and inhomogeneous dielectric structure. These inhomogeneities are impurities, grain structure and pores.

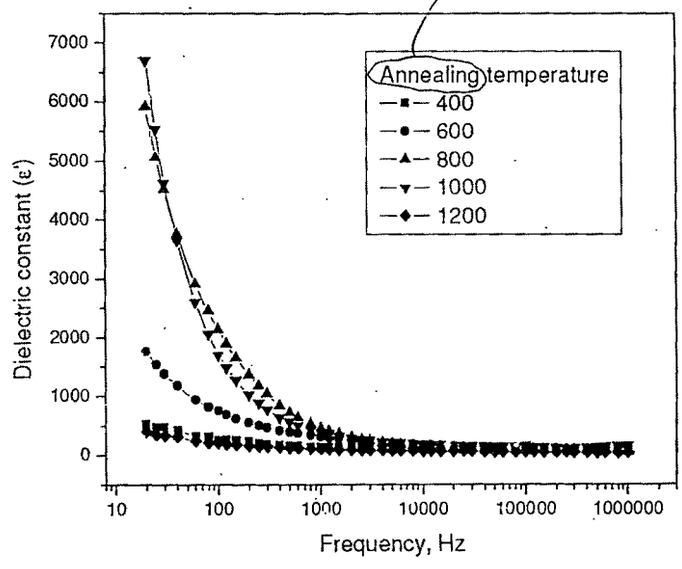

Figure 4.3 Variation of room temperature dielectric constant with frequency

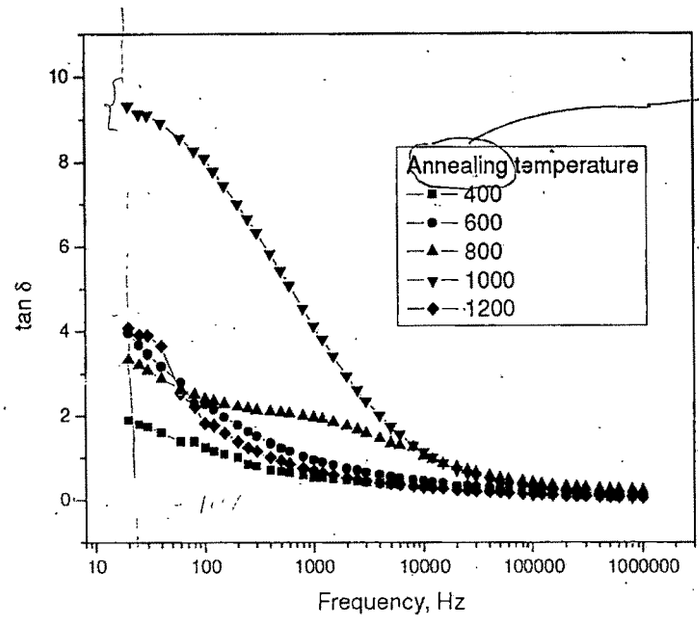

Figure 4.4 Variation of dielectric loss with frequency

The variation of dielectric loss with frequency is shown in fig. 4.4. At lower frequencies tan δ is large and it decreases with increasing frequency. The tan δ is the energy dissipation in the dielectric system, which is proportional to the imaginary part of dielectric constant. At higher frequencies the losses are reduced and the dipoles contribute to the polarization [12]. The loss factor curve is attributed to domain wall resonance. At higher frequencies, losses are found to be low if domain wall motion is inhibited and magnetization is forced to change by rotation.

To confirm the conduction mechanism in these composites, the variation of log σ_{ac} with log ω was studied [Fig. 4.5].

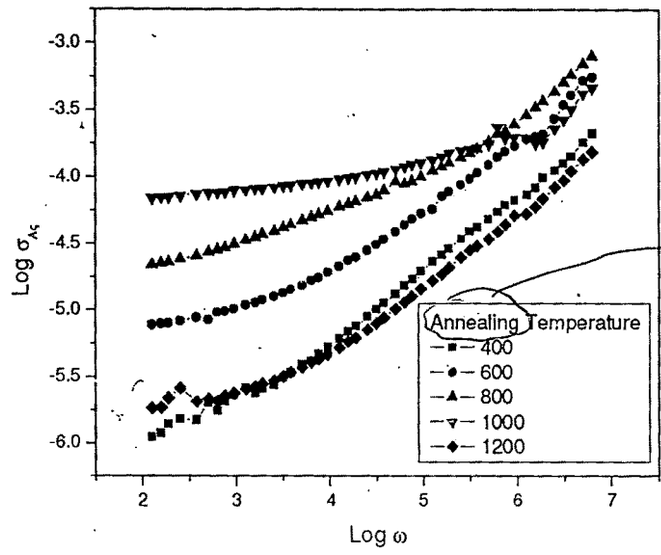

Figure 4.5 Variation of AC conductivity with frequency

The plots are observed to be almost linear indicating that the conduction increases with increase in frequency. The linearity of the plots confirms small polaron mechanism of conduction. The slight decrease in conductivity is attributed to conduction by mixed polarons. In ionic solids the electrical conductivity is due to migration of ions and the ionic transport depends on angular frequency. Thus, the ac conductivity (σ_{ac}) is proportional to the angular frequency and it is confirmed here by linear plots of conductivity with angular frequency [13]. Relatively higher value of dielectric constant, loss tangent and ac conductivity in case of the sample sintered at 1000°C might be due to dominance of Cd_2SnO_4 phase in the formed composite.

4.3.4 Electrical resistivity

Figure 4.6 shows the variation of dc resistivity with temperature. The plots show two regions of conductivity. The resistivity decreases with increase in temperature suggesting semiconductor behaviour of the samples. Slight increase in

resistivity with increase in temperature from 400 to 500°C for the samples sintered at 600, 800 and 1200°C, might be due to phase transformation during heating. The first region observed at lower temperatures is due to impurities and the second region that occurs at higher temperature is due to polaron hopping. In the hopping mechanism electrons can 'hop' from one site to another by acquiring the necessary activation energy. Such a thermally activated hopping process is possible at sufficiently high temperatures [14].

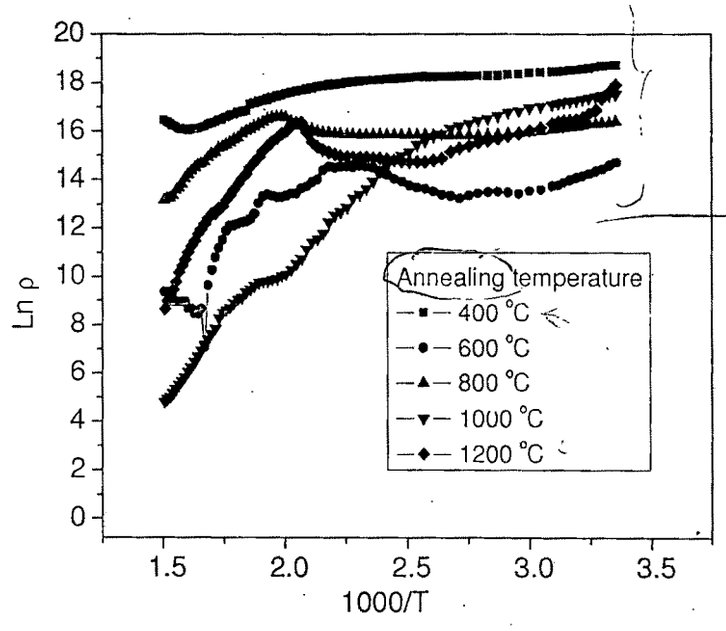

Figure 4.6 variation of dc resistivity with temperature

The dc resistivity decreases with increasing temperature because with the addition of thermal energy, electron could be set free from O^{2-} ions. When an electron is introduced in the sample it might be associated with cations, which results in an unstable valence state [15]. As the sintering temperature increases, the resistivity goes on increasing up to 1000°C and then decreases. This may be attributed to the difference

in the resistivity of two phases. The resistivity of composite is an effective value of resistivity of its constituent phases. The maximum resistivity observed at 1000°C is perhaps due to the addition of resistivities of constituent phases. The increase in resistivity of the composites as compared to constituent phases may be ascribed to the serial arrangement of grains.

The activation energy was calculated by using the relation (2.35). Activation energy in low temperature region is of the order of 0.1eV and that in the high temperature region varies from 0.26 eV to 1.13 eV. The respective values of activation energies for the samples sintered at 400, 600, 800, 1000, and 1200°C are 0.266, 0.919, 0.524, 0.933 and 1.132 eV as shown in figure 4.7.

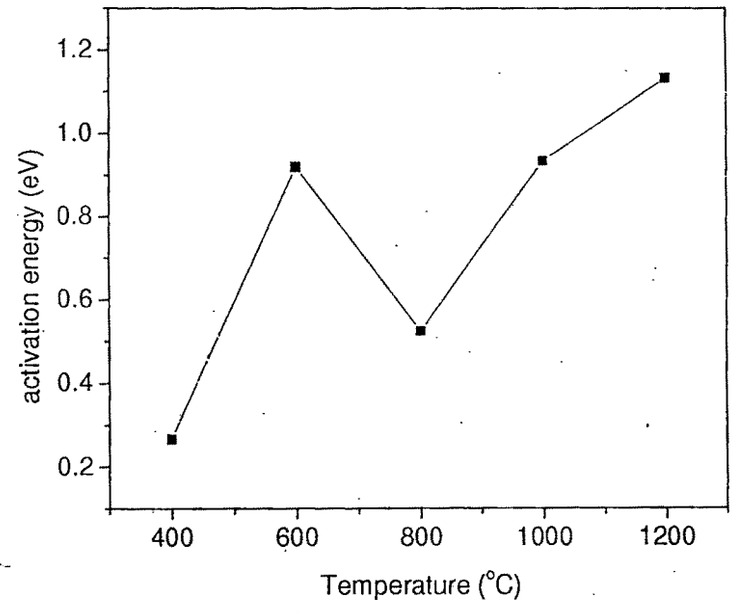

Figure 4.7 variation of activation energy with annealing temperature

References

[1] R.D. Shannon, J.L. Gillson, R.J. Bouchard, J. Phys. Chem. Solids 38 (1977) 877

[2] C.M. Cardile, R.H. Meinhold, K.J.D. MacKenzie, J. Phys. Chem. Solids 48 (1987) 881

[3] X. Jia, H. Fan, X. Lou, J. Xu, Appl Phys A, 94(2009)837

[4] W.L. Wang, K.J. Liao, C.Z. Cai, G.B. Liu, Y. Ma, Surf. Coatings technol., 167 (2003) 284

[5] R. Mamazza Jr., D. L. Morel, C. S. Ferekides, Thin Solid Films 484 (2005) 26

[6] A. J. Nozik, Phys. Rev. B 6 (1972) 453

[7] T. Hashemi, J. Illingworth, F. Golestaniford, J. Am. Ceram. Soc. 74(1991)662

[8] G. Valincius, V. Reipa, V. Vilker, J. T. Woodward, M. Vaudin, J. Electrochem.soc.148 (2001) E341

[9] J.C. Maxwell, "Electricity and Magnetism", Oxford Uni. Press, Landon, 1993, p. 828

[10] K.W. Wagner, Ann. Phys. 40 (1993) 818

[11] C.G. Koop, Phys. Rev. B 83 (1951) 121

[12] D.C. Agrawal, Asian J. Phys. 6 (1997) 108

[13] K.K. Patankar, S.S. Joshi, B.K. Chougule, Phys. Lett. A 346 (2005) 337

[14] H.V. Keer, Principles of the Solid State, New Age Int. Pub. Ltd, Mumbai, 2000, p178

[15] R. Rai, N.C. Soni, S. Sharma, R.N.P. Choudhary, in: A.P. Tandon (Ed), "Ferroelectrics and Dielectrics", Allied Publishers Pvt. Ltd., New Delhi, 2004, p. 177